

Micromechanical detectors for local field measurements based on ferromagnetic resonance (invited)Albrecht Jander, John Moreland,^{a)} and Pavel Kabos*National Institute of Standards and Technology, Boulder, Colorado 80305-3337*

Ferromagnetic resonance (FMR) measurements were performed on micrometer-size thin-film samples deposited onto a micromechanical cantilever detector. The FMR response is coupled to cantilever motion in one of three ways: (1) By measuring the change in torque on the sample in a uniform field; the FMR precession reduces the static magnetic moment of the sample with a resultant change in torque. (2) By measuring the damping torque acting on the FMR precession. (3) By measuring the energy absorbed in FMR using a bimaterial cantilever as a calorimeter sensor. Our instrument is capable of measuring the FMR response in permalloy samples as small as $2 \times 10^{-11} \text{ cm}^3$ in ambient conditions with a signal-to-noise ratio of 100. In addition we demonstrate that this system can be used as a quantitative scanning probe magnetic field microscope. Using the magnetic field sensitivity of the FMR response in a small ferromagnetic particle, we have achieved 50 A/m field resolution on 20 μm length scales. Both dc fields and microwave fields were imaged. [DOI: 10.1063/1.1354583]

INTRODUCTION

Ferromagnetic resonance (FMR) is an important experimental method for characterizing magnetic materials. Magnetic quantities such as the Lande g factor, the FMR linewidth, the anisotropy field, and the magnetization can be obtained from FMR measurements.¹ Traditional microwave cavity FMR experiments on thin films are limited in their sensitivity and require fairly large sample areas on the order of 1 mm². Recent developments in micromechanical detection of magnetic resonance using micromachined cantilever detectors have shown that it is possible to measure magnetic resonance effects in micrometer and submicrometer sized particles.²⁻⁶ Most of these techniques couple the magnetic response into a force on the cantilever by means of a strong field gradient. Here we present two techniques for micromechanical detection of FMR using the torque sensitivity of cantilevers^{7,8} and a third technique based on calorimetry.⁹ In all three cases, coupling to the cantilever motion is achieved without a field gradient.

In addition to investigating magnetic material properties, the ferromagnetic resonance effect in small particles may be used as a high-resolution probe of local magnetic fields. By attaching it to the end of a micromachined cantilever, the probe particle can be moved in space to map microscopic field distributions. Since FMR is sensitive to both the dc bias field as well as the high-frequency pumping field, both static and microwave field distributions can be imaged.

In the experiments described here, we detect the occurrence of ferromagnetic resonance through the mechanical effect on a micromachined Si cantilever. We will consider

three distinct effects: (1) The reduction of the static magnetization when FMR conditions are met. This is detected as a change in the magnetostatic torque acting on the sample in a magnetic field. (2) The damping torque. The resonance is limited by damping processes, which produce a counter-torque on the precessing spins. We measure this damping torque as a corresponding torque on the sample. (3) The energy absorbed in FMR. Excitation of FMR results in the absorption of microwave energy by the spin system. We detect the heating of the sample associated with this absorption by using the cantilever as a bimaterial calorimeter.

ANALYSIS OF MECHANICAL RESPONSES

FMR is achieved by saturating a ferromagnetic sample with a bias field and then perturbing the magnetization with a high-frequency pumping field applied perpendicular to the bias field. With the bias field applied in the z direction, the equilibrium position of the magnetization vector is also in the z direction. A harmonic pumping field h_x applied to the sample results in deviation from equilibrium given by

$$m_x = \chi h_x, \quad (1)$$

$$m_y = i\kappa h_x. \quad (2)$$

Here, $\chi = \chi' + i\chi''$ and $\kappa = \kappa' + i\kappa''$ are complex susceptibilities that can be derived from Landau-Lifschitz dynamics:¹⁰

$$\chi = \frac{\omega_m(\omega_y + i\alpha\omega)}{\omega_x\omega_y - \omega^2 + i\alpha\omega(\omega_x + \omega_y)}, \quad (3)$$

$$\kappa = \frac{-\omega_m\omega}{\omega_x\omega_y - \omega^2 + i\alpha\omega(\omega_x + \omega_y)}, \quad (4)$$

^{a)}Electronic mail: moreland@boulder.nist.gov

where ω is the angular frequency of the driving field, α is the Gilbert damping parameter, and ω_m , ω_x , and ω_y are determined by the shape and magnetization of the sample through

$$\omega_m = \gamma M_s, \quad (5)$$

$$\omega_{x,y} = \gamma [H_0 + M_s(N_{x,y} - N_s)]. \quad (6)$$

Here H_0 is the bias field, M_s is the saturation magnetization, γ is the gyromagnetic ratio, and $N_{x,y,z}$ are the demagnetizing factors of the sample.

For a sample with small damping ($\alpha \ll 1$) near resonance ($\omega^2 = \omega_x \omega_y$), the imaginary parts dominate both χ and κ , so we may write

$$m_x = i\chi'' h_x, \quad (7)$$

$$m_y = \kappa'' h_x. \quad (8)$$

This describes an elliptical precession of the magnetization with the x component out of phase with the driving field and the y component in phase with the driving field. Near resonance,

$$\chi''_{xx(\text{res})} = \frac{-\omega_m \omega_y}{\alpha \omega (\omega_x + \omega_y)} = \frac{-M_s \sqrt{1 + M_s/H_0}}{\alpha (2H_0 + M_s)}, \quad (9)$$

$$\kappa''_{(\text{res})} = \frac{\omega_m}{\alpha (\omega_x + \omega_y)} = \frac{M_s}{\alpha (2H_0 + M_s)}, \quad (10)$$

where the right-hand expressions are for the case of a thin-film sample with in-plane driving field ($N_x = N_z = 0$, $N_y = 1$).

With these standard relations, we derive the magnitude of the three effects described above. First, consider the change in magnitude of the z component of the magnetization. In the absence of a driving field, h_x , the magnetization vector lies in its equilibrium position in the z direction. When FMR is excited, the precession causes the magnetization vector to tip away from the z axis. If the magnitude of the magnetization vector remains constant, geometrical considerations lead to the result that, for small precession angles, the average value of M_z changes by⁸

$$|\Delta M_z| = \frac{|m_x|^2 + |m_y|^2}{2M_s} = \frac{M_s h_x^2}{2\alpha^2 (2H_0 + M_s) H_0}. \quad (11)$$

In the presence of a torque field H_T directed in the y direction, this change in magnetization results in a proportional change in the magnetostatic torque,

$$\Delta T_{\text{static}} = \mu_0 \frac{H_T}{H_0} \frac{M_s}{2\alpha^2 (2H_0 + M_s)} h_x^2 V. \quad (12)$$

This torque is directed in the x direction, causing a twisting about the axis of the rf field as shown in Fig. 1(a). The torque of Eq. (12) is produced by an interaction of the dc component of the magnetic moment with a static torque field.

We now turn to a different source of torque on the sample, one produced by the interaction of the oscillating field h_x with the precessing component of the magnetization. The elliptical precession of the magnetization results in a

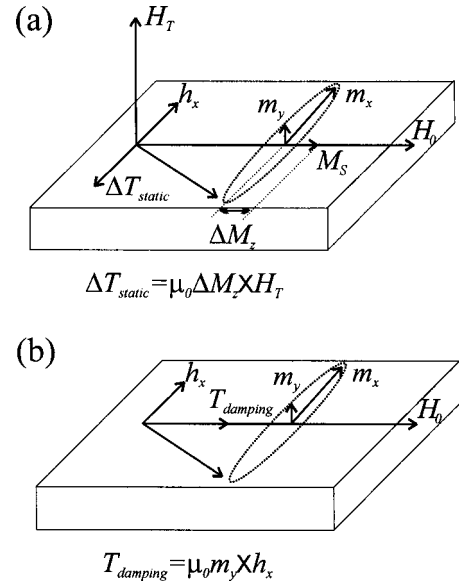


FIG. 1. Illustration of the direction of applied fields and resulting torques for (a) the magnetostatic torque in a perpendicular field and (b) the damping torque.

component of the dynamic magnetization m_y , that is perpendicular to h_x , resulting in a torque $\bar{T} = \mu_0 \bar{m} \times \bar{h}$ with an average magnitude

$$T_{\text{damping}} = \frac{1}{2} \mu_0 \kappa'' h_x^2 V \quad (13)$$

$$= \frac{\mu_0 M_s}{2\alpha (2H_0 + M_s)} h_x^2 V. \quad (14)$$

This is the torque that the microwave field exerts on the magnetization to maintain the precessional motion in the presence of damping. At steady state, this same torque must be transferred to the lattice through the damping processes. The resulting torque will tend to twist the sample about the z axis in the same direction as the precession, as indicated in Fig. 1(b).

Finally, we consider the power absorbed due to the phase lag of the magnetization m_x with respect to the driving field h_x . The phase lag is 90° at resonance and produces an oval on the m_x versus h_x plot and a corresponding power dissipation,

$$P = \frac{1}{2} \mu_0 \omega \chi''_{xx} h_x^2 V \quad (15)$$

$$= \frac{\mu_0 M_s \gamma (H_0 + M_s)}{2\alpha (2H_0 + M_s)} h_x^2 V. \quad (16)$$

As before, in the steady state, the power absorbed by the spin system must be transferred to the lattice as heat.

EXPERIMENT

The detection of the three effects described by Eqs. (12), (14), and (16) is based on the mechanical response of a micro-machined Si cantilever. The cantilever used in the present study has width $w = 49 \mu\text{m}$, length $l = 449 \mu\text{m}$, and thickness $t = 2.5 \mu\text{m}$. These cantilevers are commonly used in

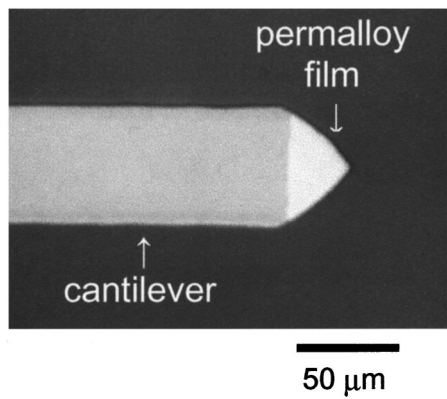


FIG. 2. Microscope photograph of the 50 nm thick permalloy sample deposited on the end of the Si cantilever. The sample volume is approximately $2.2 \times 10^{-11} \text{ cm}^3$.

atomic force microscopy (AFM). The ferromagnetic sample is deposited onto the end of the cantilever by thermal evaporation using a shadow mask to restrict deposition to only the very end of the cantilever. An optical micrograph of the 50 nm thick permalloy sample used in the experiments is shown in Fig. 2. The sample has a total volume of $2.2 \times 10^{-11} \text{ cm}^3$.

The instrumentation used to measure the mechanical response of the cantilever is shown schematically in Fig. 3. The detector system, based on a commercial AFM head, uses a laser-beam-bounce method to determine both the deflection and torsion of the cantilever. The laser is focused onto the end of the cantilever and the deviation of the reflected beam is measured in two axes by means of a four-quadrant photodiode detector.

To establish conditions for ferromagnetic resonance, the cantilever is suspended over a microwave stripline resonator driven at 8.95 GHz. The tip of the cantilever carrying the sample film is positioned above the center of the stripline where the microwave magnetic fields are directed as shown by h_x in Figs. 4(a) and 4(b). The microwave source is amplitude modulated to obtain an oscillating mechanical response of the cantilever. The response is detected by means of a lock-in amplifier synchronized with the modulating signal. For optimum sensitivity, the modulating frequency is

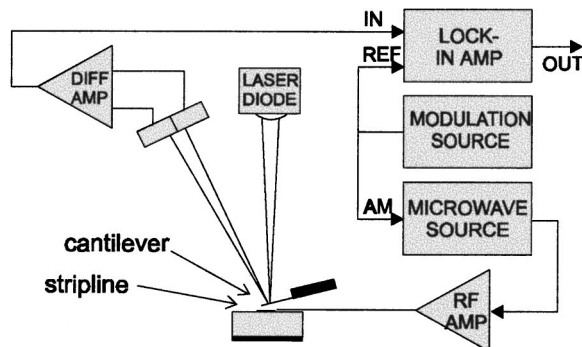


FIG. 3. Block diagram of the instrumentation used for micromechanical detection of FMR.

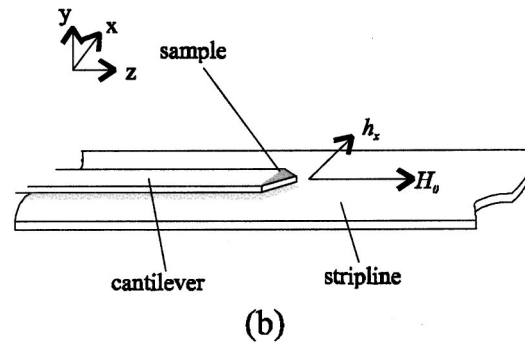
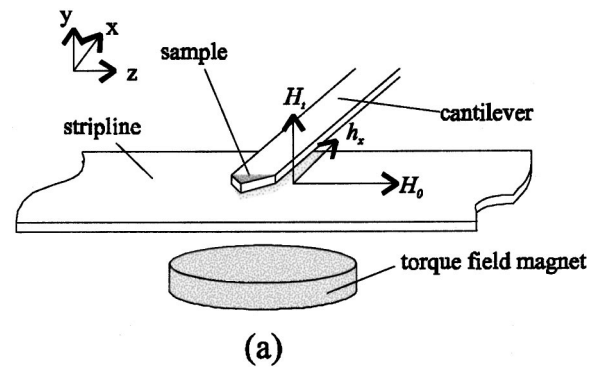


FIG. 4. Orientation of the cantilever and thin-film sample with respect to h_x from the stripline and the bias field H_0 for (a) magnetic moment torque detection and (b) damping torque detection. For calorimetry detection the configuration in (b) was used.

matched to the mechanical resonance frequency of the cantilever. The uniform bias field H_0 is applied by a dipole electromagnet surrounding the AFM.

In response to a torque on the sample about the long axis of the cantilever, the cantilever will twist according to its torsional spring constant established from elastic theory.¹¹ For a beam with $t \ll w$, the torsional spring constant is given by

$$k = \frac{T}{\phi} = \frac{Gwt^3}{3l}, \quad (17)$$

where G is the shear modulus of the cantilever material and ϕ is the torsion angle at the free end of the beam in response to a torque T . With $G = 50 \text{ GPa}$ for Si, the cantilevers used in these experiments have a torsional spring constant of approximately $3 \times 10^{-8} \text{ N m/rad}$. The torsional resonance frequency of the cantilever was $f_0 = 242.9 \text{ kHz}$ with a Q of approximately 250 in air.

The primary source of noise in these detectors is the thermomechanical vibration of the cantilever. For the torsional mode, the rms thermal noise level is found from

$$T_{\text{noise}} = \sqrt{\frac{4k_B k_B T_{\text{amb}}}{Qf_0}}, \quad (18)$$

where B is the detector's bandwidth, k_B is Boltzmann's constant, and T_{amb} is the ambient temperature. The detector bandwidth, determined by the time constant of the lock-in amplifier, was 5 Hz. For our cantilever, this specifies a noise floor of $4.5 \times 10^{-18} \text{ N m}$.

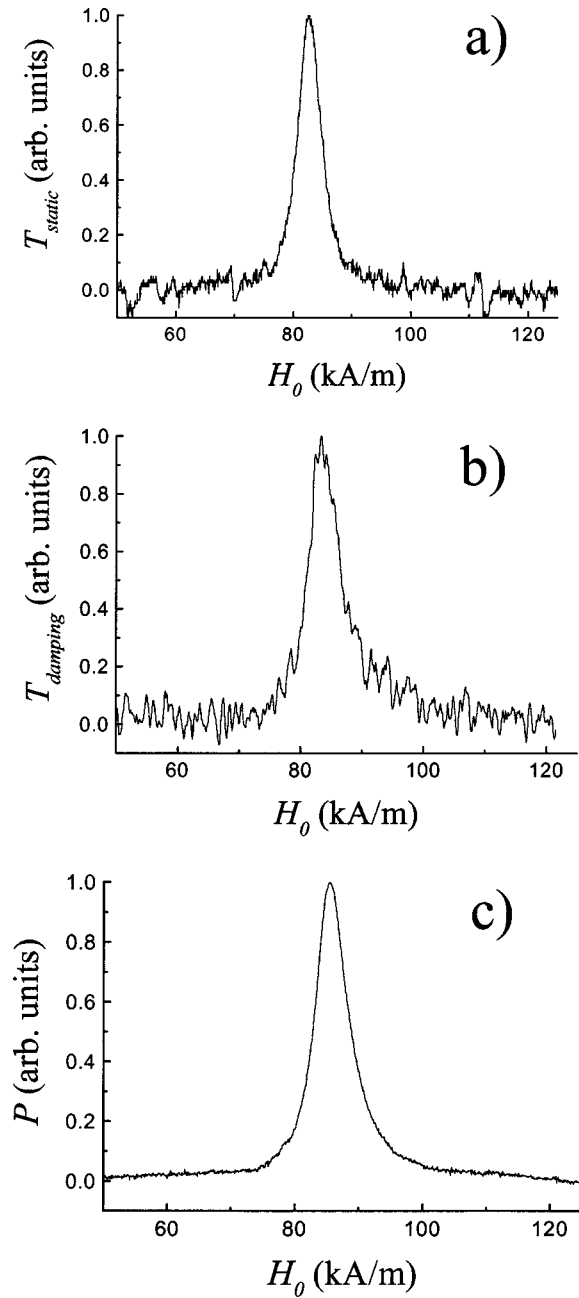


FIG. 5. FMR spectra for the $2.2 \times 10^{-11} \text{ cm}^3$ thin-film permalloy sample obtained by the three techniques: (a) magnetic-moment torque, (b) damping torque, and (c) calorimetry.

For the magnetostatic torque experiment, the cantilever was positioned with respect to the stripline as shown in Fig. 4(a). The bias field H_0 establishes a magnetization in the film perpendicular to the cantilever axis. The magnetostatic torque on the sample in the presence of the torque field H_t from the permanent magnet then has the proper orientation to apply a twisting moment to the end of the cantilever. At FMR, this torque will then be reduced by an amount ΔT_{static} , as indicated in Eq. (12). The FMR response as a function of H_0 is plotted in Fig. 5(a). With the experimental conditions, $H_0 = 85.4 \text{ kA/m}$, $H_T = 10 \text{ kA/m}$, $\alpha = 0.01$, $M_s = 672 \text{ kA/m}$, and $h_x = 200 \text{ A/m}$, Eq. (12) predicts a peak ΔT of $5.3 \times 10^{-16} \text{ N m}$, with a signal-to-noise ratio of greater than 100.

To measure the damping torque, the cantilever was repositioned as shown in Fig. 4(b) so that the precession and resulting torque is about the axis of the cantilever. A similar technique has been used to measure the damping torque in paramagnetic resonance.¹² A plot of the damping torque as a function of H_0 is shown in Fig. 5(b). With the same conditions as before, using Eq. (14) we arrive at a peak torque of $4.4 \times 10^{-17} \text{ N m}$, in rough agreement with the experiment. The signal-to-noise ratio is also close to the expected value of 10.

After completing the torque experiments, we deposited a 50 nm thick layer of Cu on the backside of the cantilever. This transforms the cantilever into a bimaterial calorimeter, which bends due to the differential thermal expansion of the Cu and Si layers. Barnes *et al.* solved the heat equation for this configuration¹³ and showed that deflection at the free end of the beam is

$$z = 2 \frac{E_1 t_1^2 l^3}{E_2 t_2^2 w} \left(\frac{\gamma_1 - \gamma_2}{\lambda_1 t_1 + \lambda_2 t_2} \right) P, \quad (19)$$

where γ , λ , t , w , l , and E are, respectively, the thermal expansion coefficient, thermal conductivity, thickness, width, length, and Young's modulus of the beam layers. The subscripts refer to the different beam layers. It is assumed that t_1 for Cu is much less than t_2 for Si and that the heat source is concentrated at the free end of the beam. For the Si cantilever described above in this experiment, with a 50 nm Cu coating, the cantilever tip displacement is calculated to be $7.2 \times 10^{-5} \text{ m/W}$.

As before, the sensitivity is limited by thermal vibration of the cantilever. The expression is similar to Eq. (18) except that the spring constant and resonance frequency for the deflection mode are used. This gives a thermal noise floor for our cantilever of approximately $x_{\text{noise}} = 3.7 \times 10^{-13} \text{ m}$, or equivalently, $P_{\text{noise}} = 5 \text{ nW}$.

Either orientation of the cantilever in Fig. 4 may be used with calorimetry detection, but the orientation of Fig. 4(b) is preferred because there is less eddy-current heating of the cantilever. The FMR spectrum determined using the calorimetry approach is shown in Fig. 5(c). The peak absorbed power, as determined from Eq. (16), is $7.7 \times 10^{-6} \text{ W}$. The predicted signal-to-noise ratio is in excess of 1000.

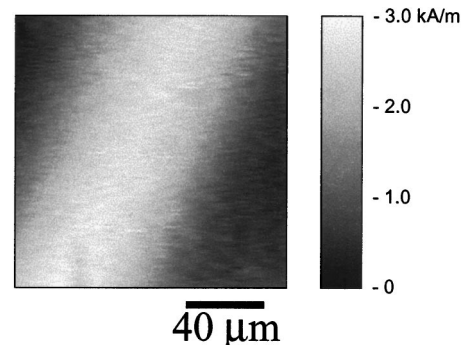


FIG. 6. Fringing fields above a $100 \mu\text{m}$ scratch in a magnetic recording medium measured by scanning FMR probe microscopy with magnetic-moment torque detection.

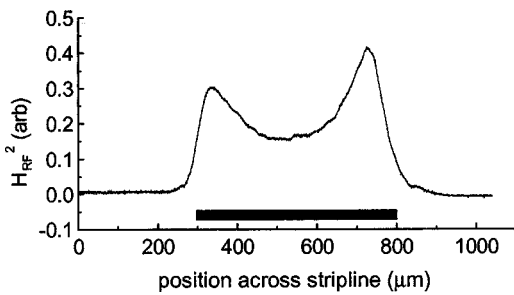


FIG. 7. Microwave power as a function of position across the stripline measured using FMR detection by micromechanical calorimetry.

APPLICATIONS AS LOCAL FIELD SENSORS

A key advantage of the cantilever-based techniques is the ability to accurately position the tip carrying the ferromagnetic sample in three dimensions using the same mechanisms typically found in atomic force microscopes. This allows the ferromagnetic response of the sample to be used as a localized field probe. Since the FMR response is sensitive to both the bias field as well as the microwave field, we can use the FMR probe both as a dc magnetic field sensor as well as a microwave power sensor. The spatial resolution of these sensors is determined by the size of the ferromagnetic particle.

We have demonstrated the ability to map an unknown field distribution using the dc torque method described above.¹⁴ The sample to be imaged is placed between the FMR probe and the stripline. The fields from the sample add to the bias field and shift the FMR response of the probe. By compensating the bias field to maintain a constant FMR response, the local fields can be determined as a function of position when the tip is scanned back and forth across the sample surface. A two-dimensional field map from the fringing fields produced by a 100 μm scratch in a FeO_x recording medium is shown in Fig. 6. The lateral resolution, as determined by the size of the ferromagnetic probe, is on the order of 20 μm . The field sensitivity, limited by thermal noise and the resonance linewidth, is approximately 50 A/m.

Alternatively, we may keep the bias field fixed and use the variation in the magnitude of the FMR response to measure spatial variations in amplitude of a microwave field. Since the peak FMR signal is proportional to h_x^2 , the resulting signal is an indication of the local microwave field intensity. Shown in Fig. 7 is the variation in FMR response, as measured by the calorimetry technique, as the probe is dis-

placed laterally across the stripline. The stripline is 500 μm wide and the tip was held approximately 50 μm above the surface of the conductor. The lateral extent of the stripline conductor is indicated in the figure, showing that the microwave field peaks near the edges of the stripline and falls off quickly as the probe moves away from the conductor.

CONCLUSIONS

We have shown FMR measurements on a sample as small as $2.2 \times 10^{-11} \text{cm}^3$ using micromechanical torque detection and calorimetry. These experiments were performed using standard Si cantilevers operating under ambient conditions. It is well-established that, based on Eq. (18), several orders of magnitude improvement in sensitivity can be achieved with custom-made cantilevers operating in vacuum.^{15,16} Cantilevers specifically designed for this purpose can have much smaller spring constants, while operating in vacuum increases the Q factor by several orders of magnitude. With this approach we expect to be able to make sensitivity improvements on the order of 10^4 , allowing FMR measurements to be made on nanometer-scale samples.

- ¹R. F. Soohoo, *Magnetic Thin Films* (Harper & Row, New York, 1965).
- ²J. A. Sidles, *Appl. Phys. Lett.* **58**, 2854 (1991).
- ³D. Rugar, C. S. Jannoni, and J. A. Sidles, *Nature (London)* **360**, 563 (1992).
- ⁴O. Züger, S. T. Hoen, C. S. Jannoni, and D. Rugar, *J. Appl. Phys.* **79**, 1881 (1996).
- ⁵Z. Zhang, P. C. Hamel, and P. E. Wigen, *Appl. Phys. Lett.* **68**, 2005 (1996).
- ⁶Z. Zhang, P. C. Hamel, M. Midzor, M. L. Roukes, and J. R. Childress, *Appl. Phys. Lett.* **14**, 2036 (1998).
- ⁷M. Löhndorf, J. Moreland, P. Kabos, and N. Rizzo, *J. Appl. Phys.* **87**, 5995 (2000).
- ⁸M. Löhndorf, J. Moreland, and P. Kabos, *Appl. Phys. Lett.* **76**, 1176 (2000).
- ⁹J. Moreland, M. Löhndorf, P. Kabos, and R. D. McMichael, *Rev. Sci. Instrum.* **8**, 3099 (2000).
- ¹⁰C. E. Patton, in *Magnetic Oxides*, edited by D. J. Craik (Wiley, London, 1975), Chap. 10.
- ¹¹J. R. Roark and W. C. Young, *Formulas for Stress and Strain*, 5th ed. (McGraw Hill, New York, 1975).
- ¹²C. Ascoli, P. Baschieri, C. Frediani, L. Lenci, M. Martinelli, G. Alzetta, R. M. Celli, and L. Pardi, *Appl. Phys. Lett.* **69**, 3920 (1996).
- ¹³J. R. Barnes, R. J. Stephenson, C. N. Woodburn, S. J. O'Shea, M. E. Welland, T. Rayment, J. K. Gimzewski, and Ch. Gerber, *Rev. Sci. Instrum.* **65**, 3793 (1994).
- ¹⁴A. Jander, J. Moreland, and P. Kabos, *Appl. Phys. Lett.* (to be published).
- ¹⁵K. Y. Yasumura, T. D. Stowe, E. M. Chow, T. Pfafman, T. W. Kenny, B. C. Stipe, and D. Rugar, *J. Microelectromech. Syst.* **9**, 117 (2000).
- ¹⁶F. R. Blom, S. Bouwstra, M. Elwenspoek, and J. H. J. Fluitman, *J. Vac. Sci. Technol. B* **10**, 19 (1992).